

# On the P-Wave Contributions to the Cross Sections of $t\bar{t}$ and $\tilde{t}\bar{\tilde{t}}$ Near Threshold

Wolfgang Mödritsch\*

Institut für Theoretische Physik  
Technische Universität Wien  
Wiedner Hauptstraße 8-10/136, A-1040 Wien  
Austria

## Abstract

The approach used for the determination of S-wave amplitudes containing the application of the nonrelativistic approximation in the case of P-waves leads to unphysical divergencies. We show how to avoid the latter in calculations of contributions to the cross section near threshold in agreement with field theory. This enables us to give quantitatively reliable predictions for the forward-backward asymmetry and for the axial contribution to the total cross section for the top-antitop system. Also the cross section for the production of stop-antistop near threshold is determined.

---

Wien, August 1995

\*E-mail: wmoedrit@ecxph.tuwien.ac.at

# 1 Introduction

The observation of the top quark has been reported recently by two collaborations at FNAL [1, 2] (CDF and D0). They quote masses of  $176 \pm 8 \pm 10 \text{GeV}$  and  $199_{-21}^{+19} \pm 22 \text{GeV}$  respectively. Electroweak data from LEP [3] and the predicted Standard Model cross section indicate a slightly lower top mass around  $170 \text{GeV}$ .

Thus it seems to be established by now that the top quark is very heavy, giving it an extraordinary status in the particle spectrum discovered so far. A main characteristic of the top quark compared to other heavy quarks is its large decay width due to  $t \rightarrow W^+ b$  of the order of  $1 \text{GeV}$ . In the present paper we will investigate properties of the top which are relevant in a future  $e^+e^-$  collider (or perhaps  $\mu^+\mu^-$ ).

Such a machine would be the ideal place to investigate in detail its properties. Especially the threshold region could give us independent determinations of the mass and width of the top quark as well as an improved determination of the strong coupling constant. Whereas for lighter quarks the  $q\bar{q}$  bound state shows individual energy levels (as in charmonium and bottomonium) the large electroweak decay width of the top smears out individual levels. On the other hand it makes QCD perturbation theory more reliable [4] because the  $t$  decays fast enough on the times scale of strong interaction to prevent hadronisation and thus essential contributions of inherent nonperturbative character.

This work is organized as follows. In sect. 2 we fix the notation for cross sections and summarize the Green function approach. Section 3 is devoted to the calculation of the forward-backward asymmetry originating in the interference of S- and P-waves. P-wave Green functions are needed exclusively for the calculation of the total cross section for the stop-antistop production as well as for the axial contribution to the cross section for  $t\bar{t}$ . Both are calculated in chapter 4. Finally in chapter 5 we draw our conclusions.

## 2 Calculation of cross sections near threshold

The nowadays quite standard Green function approach [5, 6, 7] relies on the observation that particles produced near threshold move relatively slow and thus one approximates the exact four point function by a nonrelativistic Green function. This Green function fulfills the equation

$$\{-\frac{\Delta}{m} + V(r) - E - i\Gamma\}\tilde{G}(\vec{r}, \vec{r}') = -\delta(\vec{r} - \vec{r}') \quad (1)$$

where  $V(r)$  is a perturbative or QCD-motivated potential. The width  $\Gamma$  has been included to treat an unstable particle. In general the total cross section for  $t\bar{t}$  production is given by ( a color factor 3 already included,  $X = A, V$  )

$$\sigma = \sigma_V + \sigma_A \quad (2)$$

$$\sigma_X = \frac{72}{P^2} \pi [c_X + d_X \rho] \text{Im}G^{XX}(P) \sigma_{\mu\bar{\mu}}, \quad (3)$$

whereas for scalar constituents, like  $\tilde{t}\tilde{t}$  (stop-antistop) from an eventual supersymmetric generalization only one contribution occurs

$$\sigma_s = \frac{72}{P^2} [c_s + d_s \rho] \text{Im}G_s(P) \sigma_{\mu\bar{\mu}} \quad (4)$$

with

$$\begin{aligned} c_X &:= (a^{(X)})^2 + (b^{(X)})^2 & c_s &= a_s^2 + b_s^2 \\ d_X &:= 2a^{(X)}b^{(X)} & d_s &= 2a_s b_s \end{aligned} \quad (5)$$

and

$$\sigma_{\mu\bar{\mu}} = \frac{4\pi\alpha_{QED}^2}{3P^2}, \quad P = 2m + E. \quad (6)$$

The Standard Model (SM) values of  $a^{(X)}, b^{(X)}$  as well as the values of the minimally supersymmetric extended Standard Model (MSSM)  $a_s, b_s$  are given by

$$a^{(V)} = q_t - \frac{v_t v_e P^2}{4s^2 c^2 z}, \quad b^{(V)} = \frac{v_t a_e P^2}{4s^2 c^2 z}, \quad (7)$$

$$a^{(A)} = \frac{a_t v_e P^2}{4s^2 c^2 z}, \quad b^{(A)} = -\frac{a_t a_e P^2}{4s^2 c^2 z}, \quad (8)$$

and

$$a_s = -q_t + \frac{\tilde{Q}_Z P^2}{2scz}, \quad b_s = -\frac{\tilde{Q}_Z a_e P^2}{2scz}, \quad (9)$$

where we used the abbreviations

$$z = P^2 - M_Z^2 + iM_Z\Gamma_Z, \quad s = \sin\theta_W, \quad c = \cos\theta_W \quad (10)$$

$$v_f = T_3^f - 2Q_f \sin^2\theta_W, \quad a_f = T_3^f \quad (11)$$

Here  $T_3^f$  is the eigenvalue of the diagonal SU(2) generator for the fermion  $f$  (e.g.  $t$  or  $e$ ) with charge  $Q_f$ . For the supersymmetric charges we use [8]

$$\tilde{Q}_\gamma = -q_t, \quad (12)$$

$$\tilde{Q}_Z = (\cos^2\theta_t - 2q_t \sin^2\theta_W)/(2sc). \quad (13)$$

The leading contributions to (2) arises from the vector coupling since it produces  $t\bar{t}$  pairs with angular momentum zero (S-waves). In the fermionic case P-waves are produced by the axial current and represent higher order correction. They contribute to  $O(\alpha_s^2)$  to the total cross section and lead to a forward backward asymmetry [9] by interfering with the vector contribution. On the contrary, for scalar particles P-waves represent the dominant contribution near threshold. The four point functions  $G^{XX}(P)$ ,  $G_s(P)$  are in the nonrelativistic approximation replaced by

$$\text{Im}G^{VV}(P) \rightarrow \frac{1}{m^2} \text{Im}\tilde{G}(0,0) \quad (14)$$

$$\text{Im}G^{AA}(P) \rightarrow \frac{4}{m^2} \text{Im} \frac{\partial}{\partial x_3} \frac{\partial}{\partial y_3} \tilde{G}(\vec{x}, \vec{y}) \Big|_{|\vec{x}| \rightarrow 0, |\vec{y}| \rightarrow 0} \quad (15)$$

$$\text{Im}G_s(P) \rightarrow \frac{1}{m^2} \text{Im} \frac{\partial}{\partial x_3} \frac{\partial}{\partial y_3} \tilde{G}(\vec{x}, \vec{y}) \Big|_{|\vec{x}| \rightarrow 0, |\vec{y}| \rightarrow 0} \quad (16)$$

While  $\text{Im}\tilde{G}(0,0)$  in eq. (14) is well behaved, the r.h.s in eqs. (15) and (16) are linearly divergent.

Before tackling this problem, let us consider the calculation of the nonrelativistic Green function. Due to its symmetry and the requirement of regularity at  $r \rightarrow \infty$  and at the

origin, the general solution of eq. (1) can be written as

$$\tilde{G}(\vec{r}, \vec{r}') = \sum_{l=0}^{\infty} g_l(r, r') \sum_{m=-l}^l Y_{lm}^*(\Omega') Y_{lm}(\Omega) \quad (17)$$

$$g_l(r, r') = \frac{g_<(r_<)g_>(r_>)}{r_<r_>}, \quad r_> = \begin{cases} r : r > r' \\ r' : r' > r \end{cases} \quad r_< = \begin{cases} r : r < r' \\ r' : r' < r \end{cases} \quad (18)$$

where  $g_<(r_<)$  and  $g_>(r_>)$  are regular solutions of the homogeneous equation

$$\left\{ \frac{\partial^2}{\partial r^2} - m(E + i\Gamma - V(r)) - \frac{l(l+1)}{r^2} \right\} g(r) = 0 \quad (19)$$

at  $r = 0$  or  $r \rightarrow \infty$ , respectively. The actual behavior of the solution  $g_<(r_<)$  (and also of the irregular one) for  $r \rightarrow 0$  depends on the potential and on  $l$ . In this work we use a one loop renormalization group improved potential, treating four flavors as massles ( $n_f = 4$ ). The bottom quark contribution is included in a pure perturbative manner.

$$V(r) = \frac{\alpha}{r[1 - \frac{(33-2n_f)\alpha}{8\pi}(\gamma + \ln \mu r)]} + \frac{\alpha^2}{4\pi r} [Ei(-rm_b e^{\frac{5}{6}}) - \frac{5}{6} + \frac{1}{2} \ln(\frac{\mu^2}{m_b^2} + e^{\frac{5}{3}})] \quad (20)$$

The color factor  $4/3$  is absorbed in the definition of  $\alpha$ :

$$\alpha := \frac{4}{3}\alpha_s = \frac{g^2}{3\pi} \quad (21)$$

In principle all other parts of the general potential derived in [11] on purely field theoretic grounds can be included as well.

Due to the presence of the width  $i\Gamma$  the behavior of  $g_>(r)$  for  $r \rightarrow \infty$  is given by

$$\lim_{r \rightarrow \infty} g_>(r) \propto e^{-a_- r} \quad (22)$$

with

$$a_- := \sqrt{\frac{m}{2}} \sqrt{-E + \sqrt{E^2 + \Gamma^2}}. \quad (23)$$

This exponential damping behavior is the origin of the infrared cut off mentioned already in [4]. Consider for simplicity the case  $E = 0$ . Then we can write

$$a_-^{-1} = \sqrt{\frac{2}{m\Gamma}} = \sqrt{\frac{E_B}{\Gamma}} r_B \quad (24)$$

where  $E_B = ma^2/2$  and  $r_B$  are the Bohr energy and the Bohr radius of the system, respectively. This formula clarifies that if the width  $\Gamma$  is approximately equal to  $E_B$  the form of the potential is only "tested" up to the order of magnitude of the Bohr radius. The situation is improved for  $E < -\Gamma$  since here we have

$$a_-^{-1} \leq \sqrt{\frac{1}{m|E|}}, \quad E < -\Gamma.$$

This relation also holds also for small  $\Gamma$  and thus the Bohr radius again becomes the relevant scale.

The matching condition for  $g_<$  and  $g_>$  is provided by the  $\delta$  distribution in eq. (1):

$$-m = g_<(r)g'_>(r) - g'_<(r)g_>(r) \quad (25)$$

Numerically it is possible to obtain the regular solution at the origin directly by imposing suitable boundary conditions. In the following we will need both S- and P-wave Green functions. For the singular solution of the former we use the following method [5, 7]. Suppose you have two solutions:  $g_<(r)$  as above and  $u_2(r)$  a solution determined by an arbitrary boundary condition. Then the solution  $g_>$  is given by

$$g_>(r) = c[u_2(r) + Bg_<(r)] \quad (26)$$

with

$$B = -\lim_{r \rightarrow \infty} \frac{u_2(r)}{g_<(r)}. \quad (27)$$

The constant  $c$  can be determined from eq. (25). For  $l = 0$  and a Coulomb-like potential at the origin we arrive with the boundary conditions

$$g_<(0) = 0 \quad (28)$$

$$g'_<(0) = 1$$

and arbitrary ones for  $u_2$  at the result

$$\tilde{G}_{l=0}(\vec{r}, 0) = \frac{m}{4\pi w} \frac{u_2(r) + Bg_<(r)}{r}, \quad (29)$$

$$w = u_2g'_< - g_<u'_2. \quad (30)$$

According to eq. (3) and (14) the total cross section is proportional to  $\text{Im}\tilde{G}(0,0)$ . With this knowledge it is possible to calculate the total cross section near threshold for any given potential  $V(r)$ . We have written a numerical routine for MATHEMATICA<sup>TM</sup> which has been checked to give the correct answer for the known Green function of a purely Coulombic potential.

Before presenting some numerical studies, a short remark on the coupling constant to be used seems in order. It is customary to take the strong coupling constant  $\alpha_s$  in the  $\overline{\text{MS}}$  scheme. Especially experimental determinations are always given in terms of  $\alpha_s^{\overline{\text{MS}}}(M_Z)$ . But in bound state calculations it is natural to use an  $\alpha_s$  defined differently. Clearly it should be possible to relate the two schemes. To avoid complications from heavy fermion masses we treat 4 flavors as massless. The difference in the bottom quark contribution can be expected to be smaller than the experimental uncertainties in  $\alpha_s$ . Therefore we ignore it in the following consideration. The quark-antiquark potential in the  $\overline{\text{MS}}$  scheme can be extracted e.g. from [10] to  $O(\alpha_s)$ :

$$\mathcal{V} = -\frac{4\pi\alpha}{\vec{q}^2} \left[ 1 - \alpha(3\pi\bar{\alpha}_0 \ln \frac{\vec{q}^2}{\mu^2} + \frac{31}{16\pi} - \frac{10n_f}{16\pi}) \right] \quad (31)$$

Comparison with the QCD potential [11] for  $n_f$  light flavors gives

$$\alpha^{BS} = \alpha_{\overline{\text{MS}}} \left( 1 - \frac{\alpha_{\overline{\text{MS}}}}{16\pi} (31 - \frac{10n_f}{3}) \right) \quad (32)$$

where  $BS$  denotes our bound state scheme used in [11]. Numerically this means that our  $\alpha$  is slightly smaller than usual which is advantageous for our perturbative calculation. For  $m_t = 180$ ,  $\alpha_s^{\overline{\text{MS}}}(M_Z) = .117 \pm 0.05$  get for a renormalization at  $\mu = 1/r_B(\mu)$

$$\mu = 18.5 \pm 1\text{GeV} \quad (33)$$

$$\alpha^{\overline{\text{MS}}}(\mu) = 0.22 \pm 0.01 \quad (34)$$

$$\alpha(\mu) = 0.19 \pm 0.01 \quad (35)$$

Remember that the above values for  $\alpha, \alpha^{\overline{\text{MS}}}$  differ by a factor 4/3 from  $\alpha_s$ .

### 3 Forward-Backward Asymmetry

The formalism used in the last section to investigate the total cross section for  $t\bar{t}$  production addressed a very suitable observable to determine the mass of the top quark. But since the total cross section at threshold is also significantly influenced by other quantities like the strong coupling constant and the top decay-width, it is necessary to have some independent observables. It was first proposed in [9] that the forward backward (FB) asymmetry would provide such a quantity. It has the additional advantage that it is independent of the absolute normalization of the cross section measurement. Thus it can be determined experimentally with high accuracy. However, treating this problem in a nonrelativistic context, one encounters unphysical divergences which made necessary the introduction of an unnatural cut-off. In this section we will show a systematic way how to avoid such divergencies.

The FB asymmetry is defined as the relative difference of the cross section for particles produced in the forward and in the backward direction, with respect to the direction of the  $e^-$  beam.

$$A_{FB} := \frac{\sigma_{FB}}{\sigma_{tot}} = \frac{\int_0^{\frac{\pi}{2}} d\theta \frac{d\sigma}{d\theta} - \int_{\frac{\pi}{2}}^{\pi} d\theta \frac{d\sigma}{d\theta}}{\sigma_{tot}} \quad (36)$$

Since the top quarks will be identified by their main decay products  $W$  and  $b$  let us consider the cross section for the process  $e^+e^- \rightarrow t\bar{t} \rightarrow bW^+\bar{b}W^-$ .

$$d\sigma_{e^+e^- \rightarrow bW^+\bar{b}W^-} = \frac{1}{2P^2} |M_A + M_V|^2 d\Phi_{W+b} d\Phi_{W-\bar{b}} (2\pi)^4 \delta(t_1 + t_2 - k_1 - k_2 - b_1 - b_2) \quad (37)$$

with the phase space factor

$$d\Phi_{W+b} = \frac{d^4 b}{(2\pi)^4} \frac{d^4 k}{(2\pi)^4} (2\pi) \Theta(k_{10}) \delta(k^2 - M^2) (2\pi) \Theta(b_{10}) \delta(b_1^2) \quad (38)$$

and a similar one for the decay of the antitop. Production of  $W^+bW^-\bar{b}$  via other channels can be treated as in [12].

$$\begin{aligned}
d\sigma_{FB} = & \left( \text{---}^V \text{---} \right) \left( \text{---}^A \text{---} \right)^* + \left( \text{---}^V \text{---} \right) \left( \text{---}^A \text{---} \right)^* + \\
& + \left( \text{---}^V \text{---} \right) \left( \text{---}^A \text{---} \right)^* + \left( \text{---}^V \text{---} \right) \left( \text{---}^A \text{---} \right)^* + \dots
\end{aligned}$$

Fig. 1

The FB asymmetry originates in the interference terms of the vector coupling ( $M_V$ ) and the axial coupling ( $M_A$ ). This is depicted in figure (1) where V indicates a vector and A an axial vector coupling, the star denotes complex conjugation. The matrix element  $M$  is essentially the vertex  $\gamma t\bar{t}$  and  $Zt\bar{t}$ . Near threshold the perturbative treatment of the Coulomb interaction is no longer valid. Instead one has to include the whole rung of Coulomb interactions, and even worse, it is necessary to include also the leading logarithmic contributions from the gluonic self energy corrections. We can sum the relevant set of graphs by means of the equation

$$\Gamma^\mu = \gamma^\mu - iKD\Gamma^\mu \quad (39)$$

for the vertex function  $\Gamma^\mu$ .  $D$  contains the unconnected fermion propagators and  $K$  represents the sum of all 2pi graphs. Comparison with the BS-Equation for the Feynman amplitudes

$$iG = -D + DKG \quad (40)$$

shows that eq. (39) has the solution

$$\Gamma_V^\mu = -iD^{-1}G\gamma^\mu \quad (41)$$

$$\Gamma_A^\mu = -iD^{-1}G\gamma_5\gamma^\mu, \quad (42)$$

where it is understood, that the two legs of  $G$  on the right hand side are connected with the  $\gamma$ -matrices and a momentum integration is performed.

We can split the matrix element into

$$\begin{aligned} M_A^i &= m_1 m_2 D \Gamma_A^i \\ M_V^i &= m_1 m_2 D \Gamma_V^i \end{aligned} \quad (43)$$

where

$$m_1 = \epsilon_\mu^{(\sigma)}(k_1) \bar{u}_\lambda(b_1) \left( -i \frac{e}{\sqrt{2} \sin \theta_W} V_{33}^* \gamma^\mu P_- \right) \quad (44)$$

$$m_2 = \epsilon_\nu^{*(\sigma')}(k_2) \left( -i \frac{e}{\sqrt{2} \sin \theta_W} V_{33} \gamma^\nu P_- \right) v_{\lambda'}(b_2). \quad (45)$$

Near threshold the propagators in  $D$  and the Green function  $G$  should be dominated by small momenta and therefore it should be possible to replace them by their nonrelativistic approximations. However, for  $D$  the approximation to  $O(\alpha)$  is needed for the axial vertex, since the zero order propagators would give zero due to  $\lambda^- \gamma_5 \gamma^i \lambda^+ = 0$ .

$$D \rightarrow S_{nr}^+ \otimes S_{nr}^- \quad (46)$$

$$S_{nr}^\pm = (\lambda^\pm - \frac{\vec{p} \vec{\gamma}}{2m}) \frac{1}{\frac{E}{2} \pm p_0 - \frac{\vec{p}^2}{2m} + i\frac{\Gamma}{2}} \quad (47)$$

This gives rise to the effective nonrelativistic axial vertex

$$\gamma_5 \gamma^i \rightarrow \frac{p^k}{2m} [\gamma^i, \gamma^k] \gamma_5 \lambda^- \quad (48)$$

We note already here that the term  $\frac{\vec{p}^2}{2m}$  introduces an additional power in  $\vec{p}$  which is not present in the relativistic propagator. Instead the factor  $\frac{p^k}{2m}$  in (48) would be replaced by  $\frac{p^k}{2E_p}$  which is finite for  $p \rightarrow \infty$ . Thus a divergence of (48) at  $|\vec{p}| \rightarrow \infty$  is really an artifact of the nonrelativistic approximation.

Using the fact that the heavy quarks are on shell up to  $O(\alpha^2)$  we can write

$$\int d\Phi_{W+b} \sum_{\sigma, \lambda} |m_1|^2 = -2 \text{Im} \Sigma(m^2) \lambda^+ + O(\alpha^2) \quad (49)$$

in agreement with [13].

From the modulus squared of the propagators we obtain a factor

$$\int \frac{dp_0}{2\pi} \left| \frac{1}{p_0^2 - \omega^2} \right|^2 = \frac{2}{\Gamma |2\omega|^2}, \quad (50)$$

$$\omega = \frac{1}{2m} (\vec{p}^2 - mE - im\Gamma) \quad (51)$$

Collecting everything from above, performing the trace in a frame where the leptons move along the z-axis we get for the FB-asymmetry

$$\sigma_{FB,\Lambda} = (c_{AV} + d_{AV}\rho) \frac{18\Gamma}{\pi^2 P^2} \int_0^\Lambda p^2 dp d\Omega_{FB} \text{Re}[G^*(\vec{p}) \int \frac{d^3 q}{(2\pi)^3} G(\vec{p}, \vec{q}) \frac{q^{(3)}}{m}] \sigma_{\mu\bar{\mu}} \quad (52)$$

where

$$c_{AV} = a^{(A)}b^{(V)} + a^{(V)}b^{(A)} \quad (53)$$

$$d_{AV} = a^{(A)}a^{(V)} + b^{(A)}b^{(V)} \quad (54)$$

$$\int d\Omega_{FB} = \int_0^{2\pi} d\varphi \left( \int_0^{\frac{\pi}{2}} d\theta - \int_{\frac{\pi}{2}}^{\pi} d\theta \right) \sin \theta \quad (55)$$

The SM values for  $a^{(X)}, b^{(X)}$  are given in (7) and (8). We introduced an intermediate cut-off  $\Lambda$  in (52) since the  $p$  integration is logarithmically divergent. It will be possible to remove it in the following. The Green function  $G(\vec{p})$  in (52) is defined by

$$G^*(\vec{p}) = \int \frac{d^3 q}{(2\pi)^3} G^*(\vec{p}, \vec{q}) = \frac{4\pi}{p} \int_0^\infty dr r \sin pr \tilde{G}_{l=0}(r, 0). \quad (56)$$

$\tilde{G}_{l=0}(r, r')$  denotes the S-wave Green function in configuration space, eq. (29). Let us now investigate the term

$$\int \frac{d^3 q}{(2\pi)^3} G(\vec{p}, \vec{q}) \frac{q^{(3)}}{m} = \frac{-i}{m} \int d^3 x e^{-ip\vec{x}} \frac{\partial}{\partial y_3} \tilde{G}(\vec{x}, \vec{y})|_{\vec{y}=0} \quad (57)$$

Using the representation (17) one can show that only P-waves ( $l = 1, m = 0$ ) contribute to the sum. Thus we need to evaluate eq. (19) for  $l = 1$ . The regular and singular solutions behave at the origin as

$$\begin{aligned} g_{<}^{l=1}(r) &\rightarrow c_{<} r^2, \\ g_{>}^{l=1}(r) &\rightarrow c_{>} \frac{1}{r}, \end{aligned} \quad (58)$$

respectively. We now construct a singular solution with  $c_{>} = 1$  out of two arbitrary solutions  $u_{p1}$  and  $u_{p2}$ :

$$g_{>}^{l=1}(r) = a_p [u_{p2}(r) - B_p u_{p1}(r)] \quad (59)$$

by means of

$$a_p := \lim_{r \rightarrow 0} r^{-1} [u_{p2}(r) - B_p u_{p1}(r)]^{-1}. \quad (60)$$

$B_p$  is determined by the requirement of regularity at infinity

$$B_p = \lim_{r \rightarrow \infty} \frac{u_{p2}(r)}{u_{p1}(r)}. \quad (61)$$

Then the condition (25) demands  $c_< = m/3$ . Performing the differentiation in the  $z$ -direction in the limit  $y \rightarrow 0$  in (57) leads to

$$\int \frac{d^3 q}{(2\pi)^3} G(\vec{p}, \vec{q}) \frac{q^{(3)}}{m} = \frac{\cos \theta}{p^2} \int_0^\infty dr \left( \frac{\sin pr}{r} - p \cos pr \right) g_>^{l=1}(r). \quad (62)$$

While the expressions (56) and (62) are well defined, it has been observed in [9] and [14] that (52) is logarithmically divergent. Thus cutoffs ( $\Lambda$ ) have been introduced to make numerical predictions possible. Since in our present case the divergence is only logarithmical, this leads to phenomenologically reasonable results. But the explanations given in these references are different and so are the cut-offs. It may, however, happen that for the comparison with experimental data with some cuts a reintroduction of some kind of cut-off will be necessary <sup>1</sup>, but we feel safer by first giving a satisfactory theoretically prediction and leaving this possibility open to the experimentalists.

In any case, the introduction of these cut-offs leads to some numerical uncertainty in the result, and is clearly unsatisfactory from the theoretical point of view. Furthermore we will see in the next section, that a similar UV-divergence occurs in the context of the stop–anti-stop production. Since this divergence is linear, a better understanding of the origin of this kind of divergencies is necessary to give a quantitative prediction.

The key point of our solution of the problem is to go back to the perturbative sum of the graphs for  $\sigma_{FB}$ . This is illustrated in figure (1).

Consider now the leading (tree) contribution in the nonrelativistic approximation (e.g. the first graph in fig. 1). In this case both S- and P-wave Green functions are replaced by

$$G(\vec{p}, \vec{p}') = \frac{(2\pi)^3 \delta(\vec{p} - \vec{p}')}{\frac{\vec{p}^2}{m} - E - i\Gamma}. \quad (63)$$

---

<sup>1</sup>The author is grateful to M.Ježabek for this information

This leads to the logarithmically divergent expression (for  $\Lambda \rightarrow \infty$ )

$$\sigma_{FB,\Lambda}^{(1),nr} = \frac{9\Gamma}{2m^3} \int d\Omega_{FB} \int_0^\Lambda dp \frac{p^3 \cos \theta}{|\frac{\vec{p}^2}{m} - E - i\Gamma|^2}. \quad (64)$$

Since the remaining graphs in fig. 1 by power counting can be shown to give finite results we conclude that the nonrelativistic approximation was not valid in the tree graph due to the extra power in  $p$  from the axial vertex. Furthermore since (64) is the only divergent contribution in the (infinite, but assumed to be convergent) sum in fig. 1 representing  $G$  we conclude that the divergent part of (52) is entirely contained in the first (free) contribution (64). We could now remove this divergence by a replacement  $p/m \rightarrow p/E_p$ , as indicated above. This, however, does not respect another qualitative difference between the exact tree contribution and its nonrelativistic approximation. Namely in the relativistic calculation the phase space is cut off when the momentum squared of one quark falls below the invariant mass of the decay products [5].

Therefore, we return, instead, to the relativistic expression for the tree contribution. Since we are dealing with a decaying particle, we will have to include the self energy contribution due to the decay in the propagator. This will in general lead to gauge dependent results, but we can use the constant on-shell width to obtain the leading contribution in the weak coupling [15].

This makes the quantities we are considering finite (for  $\Gamma \rightarrow 0$ ) and gauge independent. The remaining higher order contributions (e.g. gauge dependent if one considers only one diagram) can be calculated perturbatively. Therefore, to leading order it seems reasonable to take the constant width approximation for the top propagator.

Since we are only investigating processes with  $t\bar{t}$  intermediate states which will give the main contribution to the cross sections, we focus on the graph shown in fig. 2. A further advantage of this method is that now the other - non resonant - graphs for the process  $e^+e^- \rightarrow W^+bW^-\bar{b}$  to leading order in the weak coupling [12] need only to be added to yield the background contribution.

Performing the straightforward calculation for the relativistic tree contribution with

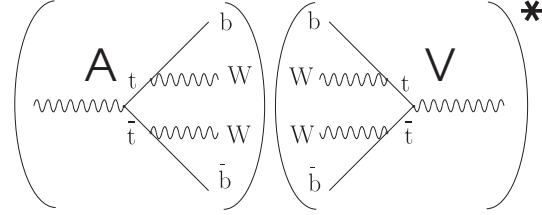


Fig. 2

a constant, but non-zero width  $\Gamma$ , we arrive at

$$\sigma_{FB}^{(1)} = \frac{18}{P^2} (c_{AV} + c_{AV}\rho) \int d\mu_1^2 \int d\mu_2^2 \Delta(\mu_1^2) \Delta(\mu_2^2) \left(1 - \frac{(\mu_1 + \mu_2)^2}{P^2}\right) \left(1 - \frac{(\mu_1 - \mu_2)^2}{P^2}\right) \quad (65)$$

where

$$\Delta(p^2) = \frac{m\Gamma}{\pi[(p^2 - m^2)^2 + m^2\Gamma^2]} \quad (66)$$

This could have been also obtained by replacing the fermion propagator by

$$S = \int d\mu^2 \frac{\Gamma}{\pi[(m^2 - \mu^2)^2 + m^2\Gamma^2]} \frac{(\not{p} + \mu)}{p^2 - \mu^2 + i\epsilon}. \quad (67)$$

and cutting it to effectively replace the phase space element for a stable quark

$$d\Phi_{stable} = \frac{d^4 p}{(2\pi)^3} \Theta(p_0) \delta(p^2 - m^2)$$

by

$$d\Phi_{unstable} = \frac{d^4 p}{(2\pi)^3} \Theta(p_0) \Delta(p^2). \quad (68)$$

A transparent summary of our approach may be formulated like this: To obtain finite, gauge independent results to the desired order we simply propose to replace the nonrelativistic tree contribution by the relativistic one and leave the (finite) rest unchanged:

$$\sigma_{FB} = \sigma_{FB}^{(1)} + \lim_{\Lambda \rightarrow \infty} (\sigma_{FB,\Lambda} - \sigma_{FB,\Lambda}^{(1),nr}) \quad (69)$$

In fig. 3 the numerical results are shown for the different contributions to  $\sigma_{FB}$  for  $\Lambda = 300$  GeV. This can be estimated to give a result for  $\lim_{\Lambda \rightarrow \infty} (\sigma_{FB,\Lambda} - \sigma_{FB,\Lambda}^{(1),nr})$  lying only 2%

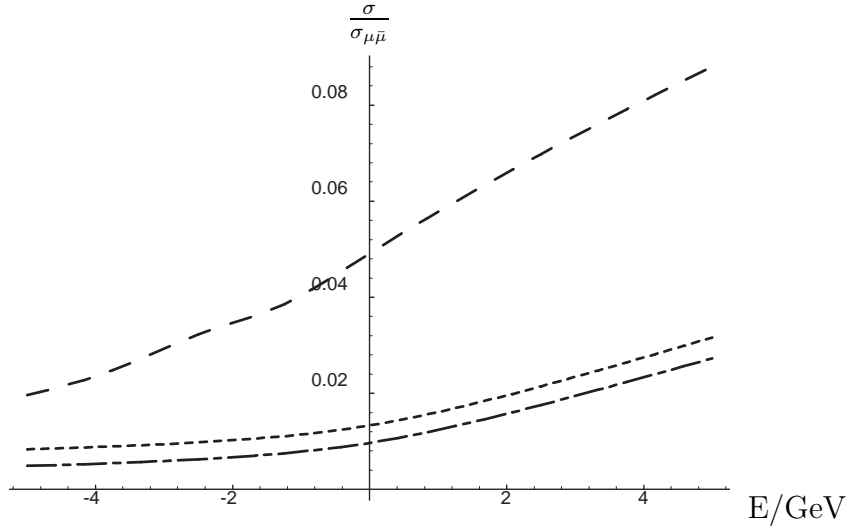


Fig. 3: Different Contributions to  $\sigma_{FB}$

dashed:  $\sigma_{FB,\Lambda}$ , dotted:  $\sigma_{FB,\Lambda}^{(1),nr}$ , dashed-dotted:  $\sigma_{FB}^{(1)}$

below the final answer. The results of the purely nonrelativistic calculations are compared to our approach in fig. 4 for  $m_t = 180$  and an electron polarization of 0.6. We also included the hard corrections as given in [14, 16].

We believe that our approach has the decisive advantage that it can be based upon to the *original* set of graphs to be considered and it is clear which graph has been calculated to which accuracy. Thus at least in principle a systematic improvement is possible. The present approach should also be applicable to the  $O(\alpha_s)$  final state corrections calculated in [17].

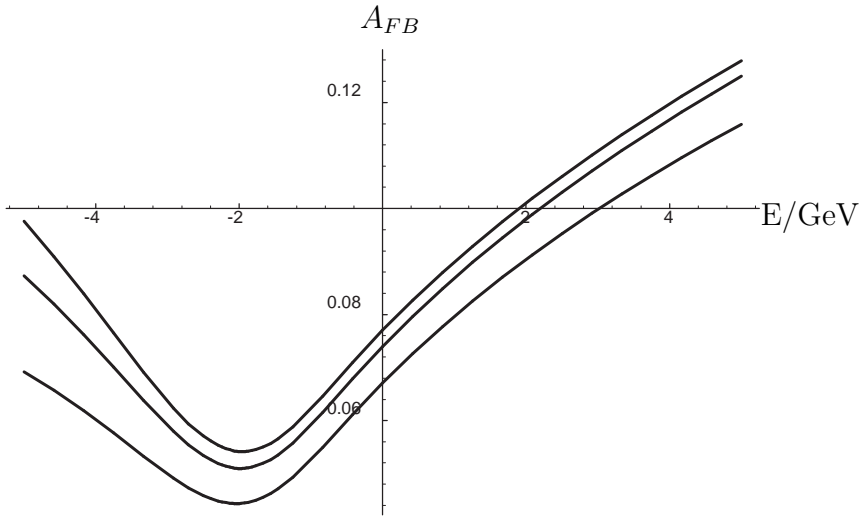


Fig. 4: Forward-backward asymmetry  $A_{FB}$ ;  
curves from top to bottom: present work, ref.[9], ref.[14]

## 4 Axial Contribution to the $t\bar{t}$ Total Cross Section and the Production of Stop-Antistop near Threshold

The total cross section for the production of P-wave states near threshold gives the leading term for the production of stop-antistop ( $t\bar{t}$ ) and a contribution of  $O(\alpha_s^2)$  to the total cross section for  $t\bar{t}$ . Only qualitative investigations on the basis of the Coulomb Green function have been published up to now [18, 19]. We will apply the method of replacing divergent nonrelativistic graphs, implicit in the Green function approach, by the relativistic, finite ones to get a reliable quantitative result also for this case.

Considering the Coulomb Green function as a first approximation it was observed in [18] that the total cross section for a stop-antistop pair near threshold develops an unphysical linear divergence due to the nonrelativistic approximation. Even a relativistic calculation of the imaginary part of the one loop contribution using the commonly used

propagator  $1/(p^2 - m^2 + im\Gamma)$  remains logarithmically divergent. This is due to the fact that this propagator does not fulfill the requirements of (local) quantum field theory as does the expression

$$\int \frac{d\mu^2}{\pi} \frac{m\Gamma}{(\mu^2 - m^2)^2 + m^2\Gamma^2} \frac{1}{p^2 - \mu^2 + i\epsilon}, \quad (70)$$

which is in agreement with the Lehmann representation of the full propagator. The tree contribution (denoted  $\sigma_1$ ) using (70) reads

$$\sigma_1 = \frac{3}{2}(c_s + d_s\rho) \int d\mu_1^2 \int d\mu_2^2 \Delta(\mu_1^2) \Delta(\mu_2^2) \Theta(P^2 - (\mu_1 - \mu_2)^2) \left[ 1 - 2\frac{\mu_1^2 + \mu_2^2}{P^2} + \frac{(\mu_1^2 - \mu_2^2)^2}{P^4} \right]^{\frac{3}{2}} \sigma_{\mu\bar{\mu}}, \quad (71)$$

whereas we have for the nonrelativistic tree contribution

$$\sigma_{1,nr}^\Lambda = \frac{3\Gamma}{\pi m^2} (c_s + d_s\rho) \int_0^\Lambda dp \frac{p^4}{(p^2 - mE)^2 + m^2\Gamma^2} \sigma_{\mu\bar{\mu}}. \quad (72)$$

However, a single subtraction of the tree graph is not sufficient. One should also subtract the logarithmically divergent one-gluon exchange term. But since we replaced the gluon propagator by the resummed one we should also calculate the relativistic graph with a resummed propagator to get the correct behavior at infinity. Unfortunately this leads to renormalon ambiguities. Therefore, we conclude that the uncertainties in choosing the right cut-off are of the same order of magnitude as higher QCD corrections, and we circumvent these difficulties for the time being by keeping the cut-off in the logarithmic divergent terms, choosing its value  $\Lambda = \Lambda_0 = m$  from the observation that this cut-off would have given the correct answer in the case of the FB-asymmetry discussed in the last section.

The same is true for the pure axial contribution to the total cross section for  $t\bar{t}$  production since each axial vertex contributes in the nonrelativistic limit an extra power in  $\vec{p}$  as explained in the last section. The only change is to replace the factor

$$f_s := \frac{3}{2}(c_s + d_s\rho) \quad (73)$$

by

$$f_f := 6(c_A + d_A\rho). \quad (74)$$

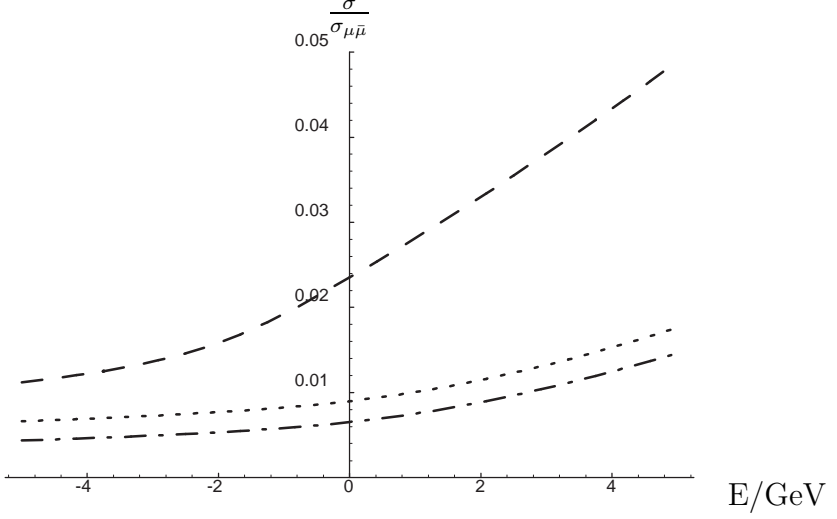


Fig. 5: Different Contributions to  $\sigma_{t\bar{t}}$

dashed: $\sigma_{nr}^{\Lambda_0}$ , dotted: $\sigma_{1,nr}^{\Lambda_0}$ , dashed-dotted:  $\sigma_{1,rel}$

Using the methods of the preceding sections we obtain within the Green function approach

$$\sigma_{nr}^{\Lambda} = f_X \frac{3\Gamma}{2\pi^2 m^2} \int_0^{\Lambda} dp p^2 \int d\Omega \left| \int \frac{d^3 q}{(2\pi)^3} \frac{q^{(3)}}{m} G(\vec{q}, \vec{p}) \right|^2 \sigma_{\mu\bar{\mu}}, \quad (75)$$

where  $f_X$  denotes either  $f_s$  for the scalar or  $f_f$  for the axial fermionic cross section. The different contributions to the cross section for the scalar case

$$\sigma = \sigma_{nr}^{\Lambda_0} - \sigma_{1,nr}^{\Lambda_0} + \sigma_1 \quad (76)$$

are depicted in fig. 5 for  $\cos^2 \theta_t = 0.5$ ,  $m = 180$ ,  $\Gamma = \Gamma_{top}$ . The net result is shown in fig. 6 for the axial contribution to the  $t\bar{t}$  cross section.

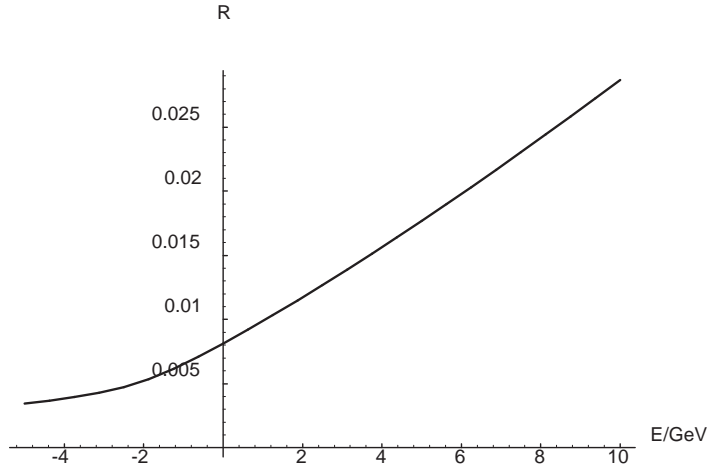


Fig. 6: Drell-ratio ( $R = \sigma_A/\sigma_{\mu\bar{\mu}}$ ) for the production of  $t\bar{t}$

The full  $O(\alpha)$  corrections are taken into account by including the hard corrections by a factor  $(1 - \frac{\alpha}{\pi})^2$  [20] and a 10% reduction of the decay width [21] in addition to the aforementioned potential. We conclude that the axial contribution gives a sizeable effect (of a few percent) to  $\sigma_{tot}$  beginning at  $\approx 5$ GeV above threshold. However, it is small enough in order to hide the uncertainty in  $\Lambda$  with respect to  $O(\alpha_s^2)$  corrections to the vector contribution to  $\sigma_{tot}$ .

In fig. 7 we compare the cross sections for the production of  $t\bar{t}$  near threshold for two different values of the decay constant ( $\cos^2 \theta_t = 0.5, m = 180$ ).

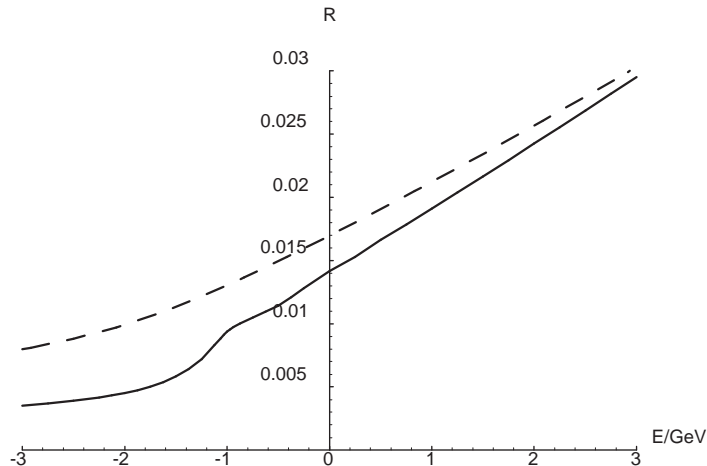


Fig. 7: dashed curve:  $\Gamma = 1.5$ GeV, full line:  $\Gamma = 0.5$ GeV

It is interesting to note that in contrast to the S-wave case the  $O(\alpha_s)$  corrections to the potential give a relatively small effect. This raises the hope that in the P-wave case fixed order perturbation theory works better as it does for S-waves and thus our subtraction procedure is strictly applicable also for the one gluon exchange term without getting troubles from the resummed gluon propagator. In fig. 8 and 9 we compare our result for the  $\tilde{t}\bar{t}$  cross section with that for a pure Coulomb potential, both computed with our subtraction method.

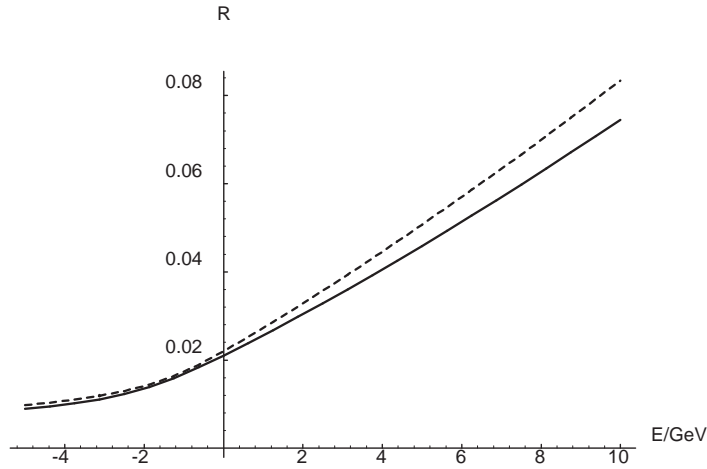


Fig. 8: dashed curve: Coulomb potential; full line: QCD-potential; both with

$$\Gamma = 1.5 \text{ GeV}$$

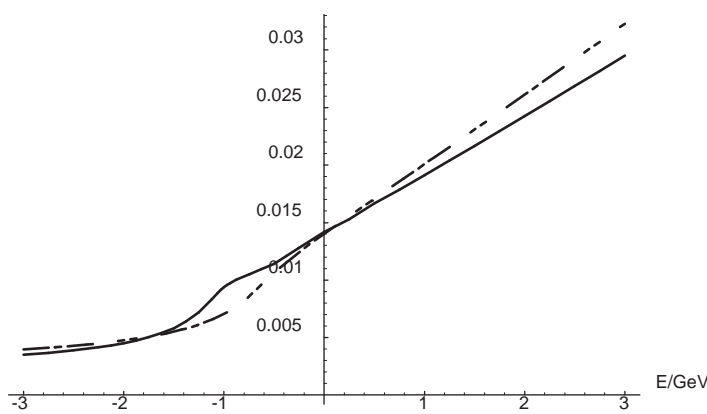


Fig. 9: dashed curve: Coulomb potential; full line QCD-potential; both with  $\Gamma = 0.5 \text{ GeV}$

A further difference is that the lowest lying resonance peak (the 2P-level) is enhanced

by the QCD potential and not suppressed as is the 1S-peak. This is in agreement with the calculation of the wave function corrections [22].

## 5 Conclusion

We have calculated the forward-backward asymmetry and the pure axial contribution to the total cross section for the  $t\bar{t}$  system. Furthermore the leading contribution to the total cross section for heavy scalars is determined in this region. Since the necessity of the inclusion of an infinite sum of Coulomb interactions in practise enforces the use of a nonrelativistic Schrödinger equation, unphysical divergencies are produced in the nonrelativistic limit. These are removed by showing that they originate in the leading nonrelativistic contributions which may be subtracted and subsequently replaced by the relativistic expressions which lead to finite results. Thus we are able to combine both the advantages of a nonrelativistic calculation near the threshold with the one of a strictly perturbative treatment.

**Acknowledgement:** This work has been supported by the Austrian Science Foundation (FWF), project P10063-PHY within the framework of the EEC- Program "Human Capital and Mobility", Network "Physics at High Energy Colliders", contract CHRX-CT93-0357 (DG 12 COMA). I am grateful to Y.Sumino for sending me the essential parts of his Fortran code for the numerical evaluation of the Green function. I am also grateful to M.Jeżabek, V.A. Khoze and J.H. Kühn for instructive discussions and to W. Kummer for a careful reading of the manuscript and many useful suggestions.

## References

- [1] F.Abe et.al. (CDF coll.):"Observation of Top Quark Production in  $p\bar{p}$  Collisions", FERMILAB-PUB-95/022-E.
- [2] S.Abach et.al. (D0 coll.):"Observation of the Top Quark", FERMILAB-PUB-95/354-E, hep-ex-9503003.
- [3] G: Altarelli:"Phenomenology in and beyond the Standard Model", CERN-TH/95-3, and references therein.
- [4] V.S. Fadin, V.A. Khoze, Sov.J. Nucl.Phys.48 (1988) 309.
- [5] Y. Sumino, K. Fujii, H. Hagiwara, H. Murayama, C.-K. Ng, Phys.Rev. D47 (1993) 56.
- [6] M. Jeżabek, J.H. Kühn, T.Teubner, Z.Phys.C56 (1992) 653; M. Jeżabek, T.Teubner, Z.Phys.C59 (1993) 669.
- [7] M.J. Strassler, M.E. Peskin, Phys.Rev.D43 (1991) 1500.
- [8] "Gluon Radiation Off Scalar Stop Particles", W.Beenaker, R.Höpker, P.M.Zerwas, DESY 94-235
- [9] H. Murayama, Y. Sumino, Phys.Rev.D 47 (1993) 82
- [10] A.Billoire, Phys.Lett.B 92 (1980) 343.
- [11] W.Kummer, W.Mödritsch, Z.Phys. C66 (1995) 225.
- [12] A. Ballestrero, E. Maina, S. Moretti, Phys.Lett. B 333 (1994) 434
- [13] W. Mödritsch, W.Kummer, Nucl. Phys. B430 (1994) 3; W.Kummer, W.Mödritsch, Phys.Lett B349 (1995) 525.
- [14] R.Harlander,M.Jeżabek,J.H. Kühn,T.Teubner,"Polarization in Top Quark Pair Production near Threshold", hep-ph/9411395, TTP94-28.
- [15] M. Veltman, Physica 29 (1963) 186, H. Veltman, Z.Phys.C 62 (1994) 35.
- [16] J.H. Kühn, P.W. Zerwas, Phys.Rep.167 (1988) 321.
- [17] Y.Sumino, Ph.D.Thesis Univ. of Tokyo, 1993, UT-655

- [18] I.I.Bigi,V.S.Fadin,V.Khoze,Nucl. Phys. B377 (1992) 461.
- [19] V.S Fadin, V.A. Khoze, Sov.J. Nucl.Phys.53 (1991) 692; (Yad.Fiz.53 (1991) 1118).
- [20] S.Güsken, J.H.Kühn, P.M.Zerwas, Phys.Lett. B155 (1985) 185;  
J.Jersák, E.Laermann, P.M.Zerwas, Phys.Rev.D25 (1982) 1218.
- [21] M.Jeżabek, J.H.Kühn, Nucl.Phys. B314 (1989) 1.
- [22] W.Kummer, G.Wirthumer, Nucl.Phys. B185 (1981) 41, E:B194(1982) 546